A STUDY OF TRANSIENT RESPONSE OF INITIALLY STRESSED COMPOSITE SANDWICH FOLDED PLATES

AK Nayak[1], RA Shenoi[2] , JIR Blake[3]

[1] Author for Correspondence, Reader, ajaya_nayak_07@yahoo.co.uk, Ph No:00919777460423, Fax No:00916632430204

[2]Professor, r.a.shenoi@soton.ac.uk

[3]Lecturer, J.I.R.Blake@soton.ac.uk

[1]Veer Surendra Sai University of Technology, Burla, 768018, Sambalpur, Odisha, India.

[2,3]University of Southampton, Highfield, SO17 1BJ, Southampton, UK.

Abstract: In this paper a C^o four node flat facetted shell element with drilling rotational degrees of freedom based on a first order shear deformation shell theory is developed to study the transient response of initially stressed composite sandwich folded plates. The new shell element contains three translations, two rotations of the normals about the shell mid-plane, and one drilling rotational degree of freedom per node. A consistent mass matrix formulation is employed to evaluate the total kinetic energy of the system. A generic validation study is carried out to evaluate the performance of the present finite element formulation. New results are presented for the transient analysis of initially stressed composite sandwich folded plate structures

Keywords: *Transient analysis; First-order shear deformation shell theory; Assumed strain concept; Folded plate structures.*

1 Introduction

Shell structures have a wide range of engineering applications in aircraft fuselages, ship hulls, buildings, bridges and vehicle chassis, among other structures. With the advent of fiber-reinforced laminated composites, the applicability of shell structures has increased many folds due to their low weight, high stiffness and high strength properties. During their build and fabrication, sandwich structures are subjected to various edge loads which can lead quickly to failure. Hence the effects of initial stresses on the dynamic response of composite sandwich shells have become an active field of applied research in recent years.

A significant amount of efforts [1-3] has been spent to study the dynamic response of laminated composite shell structures. Irie et al [4] employed the Rayleigh-Ritz method based on the Kirchhoff-Love theory to calculate the natural frequencies and mode shapes of a cantilever folded plate. Liu and Huang [5] developed the finite element transfer matrix method based on the classical plate theory (CPT) to study the natural frequencies of cantilever folded plates and shell panels. Cheung and Kong [6] used spline finite strip method to analyse folded plate structures. The displacement function of a flat shell finite strip is made up of two parts, namely the two in-plane displacement interpolations and the out-of-plane displacement interpolation. Each of the three displacement components is interpolated by a set of computed shape functions in the longitudinal direction and, as usual, one-dimensional shape functions in the transverse direction. Only standard beam shape functions are involved in the longitudinal computed shape functions. The computation of the stiffness matrix involves no numerical integration. Daniel et al [7] investigated the impact response of plate with stringers and thin walled box beams utilising a spectral element method. The results were verified with the finite element model based on a

combination of Discrete Kirchhoff Triangle (DKT) plate element and constant strain triangular element (CST) with drilling degrees of freedom. Allman [8] devised a triangular flat facet finite element incorporating the bending and membrane consistent mass matrices to analyse the free vibration response of folded plate structures. To the best of the author's knowledge, the work of Allman [8] is one of the few attempts to incorporate consistent mass matrix containing rotary inertia terms in an element formulation. Suresh and Malhotra [9] used a four node plate bending element with drilling degrees of freedom based on a first order shear deformation theory to determine the natural frequencies and modal loss factors of box beams. Niyogi et al [10] analysed composite folded plate structures using a nine node plate bending element with drilling degree of freedom based on a first order shear deformation theory. Lee et al [11] predicted the dynamic behaviour of folded composite plates by using a four node plate bending element with drilling degree of freedom based on a third order shear deformation theory. Subsequently Lee and Wooh [12] extended their earlier idea to analyse the free vibration response of composite box beams. Rao et al [13] performed experiments on initially stressed damped sandwich beams along with a finite element formulation to determine the natural frequencies and loss factors. More recently the present authors [14-15] presented results for the natural frequencies of undamped and damped composite sandwich shells using flat facetted higher order shell elements.

From a literature review, apart from the earlier works [13], which deals with damping analysis of initially stressed sandwich panels, the dynamic behaviour of initially stressed composite sandwich shells which arise in many practical situations has received very little attention. In the present study, a four node assumed strain shell element is developed based on a first order shear deformation theory having six degrees of freedom per node to analyse the transient response of initially stressed composite sandwich folded plate structures.

2 Finite Element Formulation

The present finite element displacement field (see Figure 1) of a new four node shell element based on a first order shear deformation theory is stated [16] as

$$u_1 = \sum_{i=1}^{4}\left(u_{oi}N_i + z\psi_{xi}N_i\right) + \left(y_{14}N_8 - y_{21}N_5\right)\theta_{z1} + \left(y_{21}N_5 - y_{32}N_6\right)\theta_{z2} + \left(y_{32}N_6 - y_{43}N_7\right)\theta_{z3} + \left(y_{43}N_7 - y_{14}N_8\right)\theta_{z4}$$

$$u_2 = \sum_{i=1}^{4}\left(v_{oi}N_i + z\psi_{yi}N_i\right) + \left(x_{41}N_8 - x_{12}N_5\right)\theta_{z1} + \left(x_{12}N_5 - x_{32}N_6\right)\theta_{z2} + \left(x_{23}N_6 - x_{34}N_7\right)\theta_{z3} + \left(x_{34}N_7 - x_{41}N_8\right)\theta_{z4}$$

$$u_3 = w_o \tag{1}$$

where u_1, u_2 and u_3 are the displacement components in the *x*, *y* and *z* directions respectively, of a generic point in the laminate space. u_o, v_o and w_o are the in-plane and transverse displacements of a point (*x,y*) on the mid-plane respectively. ψ_x and ψ_y are the rotations of normal to the mid-plane about *y* and *x* axes respectively. θ_{zi} (*i*=1,4) are the drilling rotations, N_i (*i*=1,4) are the shape functions, $x_{ij} = x_i - x_j$ and $y_{ij} = y_i - y_j$ are corner coordinate differences, and the shape functions N_i (*i*=5,8) associated with drilling rotations [16] are

$$N_5 = \frac{1}{16}\left(1-\xi^2\right)\left(1-\eta\right) \quad N_6 = \frac{1}{16}\left(1+\xi\right)\left(1-\eta^2\right)$$

$$N_7 = \frac{1}{16}\left(1-\xi^2\right)\left(1+\eta\right) \; N_8 = \frac{1}{16}\left(1-\xi\right)\left(1-\eta^2\right) \tag{2}$$

where ξ and η are the usual iso-parametric coordinates.

The strains associated with the displacements in Equation (1) are

$$\varepsilon_1 = \varepsilon_1^o + z\kappa_1^o, \varepsilon_2 = \varepsilon_2^o + z\kappa_2^o, \varepsilon_3 = 0, \varepsilon_4 = \varepsilon_4^o, \varepsilon_5 = \varepsilon_5^o, \varepsilon_6 = \varepsilon_6^o + z\kappa_6^o \tag{3}$$

where $\varepsilon^o = \left(\varepsilon_1^o, \varepsilon_2^o, \varepsilon_6^o\right)^T = \left(\frac{\partial u_{do}}{\partial x}, \frac{\partial v_{do}}{\partial y}, \frac{\partial u_{do}}{\partial y} + \frac{\partial v_{do}}{\partial x}\right)^T$

$$u_{do} = \sum_{i=1}^{4}\left(u_{oi}N_i\right) + \left(y_{14}N_8 - y_{21}N_5\right)\theta_{z1} + \left(y_{21}N_5 - y_{32}N_6\right)\theta_{z2} + \left(y_{32}N_6 - y_{43}N_7\right)\theta_{z3} + \left(y_{43}N_7 - y_{14}N_8\right)\theta_{z4}$$

$$v_{do} = \sum_{i=1}^{4}\left(v_{oi}N_i\right) + \left(x_{41}N_8 - x_{12}N_5\right)\theta_{z1} + \left(x_{12}N_5 - x_{23}N_6\right)\theta_{z2} + \left(x_{23}N_6 - x_{34}N_7\right)\theta_{z3} + \left(x_{34}N_7 - x_{41}N_8\right)\theta_{z4}$$

$$\kappa^o = \left(\kappa_1^o, \kappa_2^o, \kappa_6^o\right)^T = \left(\frac{\partial \psi_x}{\partial x}, \frac{\partial \psi_y}{\partial y}, \frac{\partial \psi_x}{\partial y} + \frac{\partial \psi_y}{\partial x}\right)^T$$

$$\varepsilon^s = \left(\varepsilon_5^o, \varepsilon_4^o\right)^T = \left(\frac{\partial w_o}{\partial x} + \psi_x, \frac{\partial w_o}{\partial y} + \psi_y\right)^T$$

The generalized mid-surface strains at any point given by Equation (3) can be expressed in terms of nodal displacements $\{\delta\}_{(e)}$ as follows:

$$\varepsilon^{o(e)} = \left[B_\varepsilon^o\right]^{(e)}\{\delta\}_{(e)}, \kappa^{o(e)} = \left[B_\kappa^o\right]^{(e)}\{\delta\}_{(e)} \text{ and } \varepsilon^{s(e)} = \left[B_\varepsilon^s\right]^{(e)}\{\delta\}_{(e)} \tag{4}$$

where $\left[B_\varepsilon^o\right]$, $\left[B_\kappa^o\right]$ and $\left[B_\varepsilon^s\right]$ are generated strain-displacement matrices. One basic problem inherent in the use of standard interpolation of the strains for the transverse shear components is that the element locks when it is thin. The reason for this locking is that the element, when loaded in pure bending, will exhibit spurious transverse shear energy. In order to overcome the shear locking, Dvorkin and Bathe [17] proposed assumed interpolations for the shear strain to develop a four node assumed strain degenerated shell element. In the present paper same shape functions are chosen to develop our new four node flat shell element with vortex rotations.

The substitute shear strain fields [17] are chosen as follows:

$$\bar{\varepsilon}^{s}_{\xi\varsigma} = \sum_{i=1}^{1}\sum_{j=1}^{2} P_i(\xi) Q_j(\eta) \bar{\varepsilon}^{sij}_{\xi\varsigma} \tag{5}$$

$$\bar{\varepsilon}^{s}_{\eta\varsigma} = \sum_{i=1}^{21}\sum_{j=1}^{1} Q_i(\xi) P_j(\eta) \bar{\varepsilon}^{sji}_{\mu\varsigma} \tag{6}$$

where $Q_1(z) = (1+z)/2$, $Q_2(z) = (1-z)/2$ and $P_1(z) = 1(z = \xi, \eta)$ in which $\bar{\varepsilon}^{sij}_{\xi\varsigma}$ and $\bar{\varepsilon}^{sij}_{\eta\varsigma}$ are the $m \times n$ unknown substitute shear strain parameters (Figure 2) associated with two sets of $m \times n$ sampling points $\left(\hat{\xi}_i, \hat{\eta}_j\right)$ and $\left(\breve{\xi}_j, \breve{\eta}_i\right)$.

In order to eliminate locking, the following equations are obtained:

$$\bar{\varepsilon}^{s}_{\xi\varsigma}\left(\hat{\xi}_i, \hat{\eta}_j\right) = \varepsilon^{s}_{\xi\varsigma}\left(\hat{\xi}_i, \hat{\eta}_j\right)\left(i = 1,....,m;\ j = 1,.....,n\right) \tag{7}$$

$$\bar{\varepsilon}^{s}_{\eta\varsigma}\left(\breve{\xi}_j, \breve{\eta}_i\right) = \varepsilon^{s}_{\eta\varsigma}\left(\breve{\xi}_j, \breve{\eta}_i\right)\left(i = 1,....,n;\ j = 1,.....,m\right) \tag{8}$$

It is possible to write

$$\bar{\varepsilon}^{s} = \begin{Bmatrix} \bar{\varepsilon}^{o}_{5} \\ \bar{\varepsilon}^{o}_{4} \end{Bmatrix} \tag{9}$$

where $\bar{\varepsilon}^{o}_{5}$ and $\bar{\varepsilon}^{o}_{4}$ are obtained from $\bar{\varepsilon}^{s}_{\xi\varsigma}$ and $\bar{\varepsilon}^{s}_{\eta\varsigma}$ given by Equations (5-6) by tensor transformation. The transformation of the strain tensor in curvilinear coordinates may be written as

$$e_{\alpha\beta} = \frac{\delta x^{i}}{\delta \varepsilon_{\alpha}} \frac{\delta x^{j}}{\delta \varepsilon_{\beta}} \varepsilon_{ij} \tag{10}$$

where it is assumed that $e_{\alpha\beta}$ is the strain tensor in the (ξ, η) coordinate system and ε_{ij} is the strain tensor in the (x, y) system. For further details, see Dvorkin and Bathe [17]. For implementation purpose, ε^{s} in Equation (4) is replaced by $\bar{\varepsilon}^{s}$ where $\bar{\varepsilon}^{s}$ is the substitute shear strains to remove spurious zero energy modes. Hence the substitute shear strain $\bar{\varepsilon}^{s}$ is given by

$$\bar{\varepsilon}^{s(e)} = \left[\bar{B}_{\varepsilon}^{s}\right]^{(e)} \{\delta\}_{(e)} \tag{11}$$

where $\left[\bar{B}_{\varepsilon}^{s}\right]^{(e)}$ is generated strain displacement matrix.

For arbitrary values of virtual displacements, the following assembled equation for transient analysis is stated as:

$$[M]\{\ddot{\Delta}\} + [K]\{\Delta\} = \{F\} + \lambda_b \left[K_g\right]\{\Delta\} \tag{12}$$

Here the unknown vector $\{\Delta\}$ is generated by the assemblage of element degrees of freedom $\{d\}_e^T$, e=1,….,total degrees of freedom in the region **R**. λ_b denotes the buckling parameter (a function of the constant inplane edge loads $\bar{N}_{xx}$, $\bar{N}_{yy}$ or $\bar{N}_{xy}$). The assembled stiffness, mass and buckling matrices for transient analysis are

$$[K] = \sum_{e} \int_{A_e} \left[B_{\varepsilon}^{oT} A B_{\varepsilon}^{o} + B_{\varepsilon}^{oT} B B_{\kappa}^{o} + B_{\kappa}^{oT} B B_{\varepsilon}^{o} + B_{k}^{oT} D B_{\kappa}^{o} + \bar{B}_{\varepsilon}^{sT} A^{s} \bar{B}_{\varepsilon}^{s} \right] dA \tag{13}$$

where $A_{ij}, B_{ij},$ etc are the plate stiffness, defined by

$$\left(A_{ij}, B_{ij}, D_{ij}\right) = \int_{-h/2}^{h/2} \bar{Q}_{ij} \left(1, z, z^2\right) dz \left(i, j = 1, 2, 6\right)$$

$$\left(A_{ij}^{s}\right) = \int_{-h/2}^{h/2} \bar{Q}_{ij} K_1^2 K_2^2 \left(1\right) dz \left(i, j = 5, 4\right) \tag{14}$$

where K_1^2 and K_2^2 are the shear correction factors [14-15, 18] calculated from the shear strain energy formulation.

$\bar{Q}_{ij}$ [25] are the transformed plane stress reduced elastic stiffness coefficients.

The consistent mass matrix $[M]$ in Equation (12) can be obtained from the kinetic energy $\left(\int_V \rho \left(\ddot{u}_1 \delta u_1 + \ddot{u}_2 \delta u_2 + \ddot{u}_3 \delta u_3 \right) dV \right)$ of the system where $\rho(x, y, z)$ and V are the density of the shell at (x, y, z) and volume of the shell respectively.

$$\left[K_g\right] = \sum_e \int_{A_e} [X]^T \left[\bar{N}\right][X] dA \tag{15}$$

where $[X] = \begin{bmatrix} N_{,x} & N_{,y} \end{bmatrix}^T$ and $\{F\}$ is the column vector containing the boundary and body force contributions. By the rules of orthogonal transformation the stiffness, mass and buckling matrices of an element in global co-ordinate become

$$[K]^g = T_g{}^T [K] T_g \tag{16}$$

$$[M]^g = T_g{}^T [M] T_g \tag{17}$$

$$\left[K_g\right]^g = T_g{}^T \left[K_g\right] T_g \tag{18}$$

where T_g is the transformation matrix [19] from local to global axes as given below

$$T_g = \begin{bmatrix} T_{gtop} & 0 \\ 0 & T_{gbot} \end{bmatrix}$$

$$T_{gtop} = \begin{bmatrix} \cos(X,x) & \cos(X,y) & \cos(X,z) \\ \cos(Y,x) & \cos(Y,y) & \cos(Y,z) \\ \cos(Z,x) & \cos(Z,y) & \cos(Z,z) \end{bmatrix}$$

$$T_{gbot} = \begin{bmatrix} \cos(Y,y) & -\cos(Y,x) & \cos(Y,z) \\ -\cos(X,y) & \cos(X,x) & -\cos(X,z) \\ \cos(Z,y) & -\cos(Z,x) & \cos(Z,z) \end{bmatrix}$$

$$0 = \begin{bmatrix} 0 & 0 & 0 \\ 0 & 0 & 0 \\ 0 & 0 & 0 \end{bmatrix}$$

and (X, x) denotes the angle between the positive X (global) and x (local) axes.

A 2 x2 Gauss-Legendre rule (i.e full integration scheme) is employed to integrate bending, membrane, shear and inertia terms in the energy expressions for our new four node drilling degrees of freedom shell element.

3 Numerical Results and Discussions

Numerical results are carried out to study a number of test problems to validate the present finite element formulation. The following boundary conditions are adopted in the analysis: Simply supported (S) (for cross ply): $u_o = w_o = \psi_x = \theta_z = 0$ at $y = 0, b$; $v_o = w_o = \psi_y = \theta_z = 0$ at $x = 0, a$; (for angle ply): $v_o = w_o = \psi_x = \theta_z = 0$ at $y = 0, b$; $u_o = w_o = \psi_y = \theta_z = 0$ at $x = 0, a$; Clamped (C); $u_o = v_o = w_o = \psi_x = \psi_y = \theta_z = 0$ at $x = 0, a$ and $y = 0, b$, where a and b are rectangular projections of the shell reference surface on the plane.

Example 1: Straight cantilever beam under end shear

This example deals with the static analysis of a straight cantilever beam [20] under shear loading. This problem serves as benchmark to evaluate the performance of shell elements with drilling rotational degrees of freedom.

The geometrical and material properties for this problem are [20]: a = 48 cm, b = 12 cm, h = 1.0 cm, E = 3.0 x 10^4 N/cm^2, ν = 0.25, shear load of 40 N at the free end. The boundary conditions are $u_o = v_o = w_o = \psi_x = \psi_y = \theta_z = 0$ at x=0. The analytical solution [20] for the displacement at

the loaded end is 0.35583 cm. The results from various mesh densities are shown in Table 1. As can be seen from the results, the present results show convergence to the analytical solution [20] on the refinement of the mesh densities.

Example 2: Scordelis-Lo roof under gravity loading

The cylindrical shell roof [17] problem shown in Figure 3, is a well known benchmark problem to assess the behaviour of shell elements. The shell is supported by rigid diaphragm at the curved edges and free at the straight edges. The shell is loaded vertically under its uniform dead weight of 90.0 per unit area (4309.2 Pa). The following material and geometrical properties [17] in consistent units are: R = 300 in (7.62 m), L = 600 in (15.24 m), E = 3.0 x 10^6 psi (20685 x 10^6 Pa), ν = 0.0, specific weight = 0.208333 lb/cubic in (56548.58 N/cubic m), thickness= 3in (0.0762 m). Because of double symmetry, only one quarter of the shell roof is discretized into 25, 100, 400 and 900 elements. The boundary conditions are adopted as mentioned in References [24, 17 and 19]. The vertical deflection at the mid-point of the free edge is normalized with the analytical solution for the deep shell solution 3.6288 in (0.09217 m) [17]. The normalized results from FSDTC4 (4 node first order shell element with shear correction factors of 5/6) from different mesh densities of 5, 10, 20 and 30 elements per side are shown in Figure 4. It is observed that the present results converge towards the exact solution on the refinement of mesh densities. The displacement profile of the shell roof from a mesh density of 30 elements per side from FSDTC4 is shown in Figure 5 along with the results from the analytical solution [21]. As expected, the present FEM results are in close agreement with the analytical solution.

Example 3: Pinched Cylinder Problem

This example includes a cylinder which is supported by two rigid diaphragms at the ends and pinched by two equal and opposite forces at the mid-span position. The geometrical and material properties [17] are: R = 300 in (7.62 m), L = 600 (15.24 m), thickness = 3.0 in (0.0762 m), E = 3.0 x 10^6 psi (20685 x 10^6 Pa), ν = 0.3 and the pinching load P = 1.0 lb (4.448 N). Only one-eighth of the cylinder as shown in Figure 6 is modeled with 25, 100, 400 and 900 elements due to the symmetry. The boundary conditions are adopted as mentioned in References [24, 17 and 19]. The comparative normalized results from FSDTC4 with the analytical solution [17,22] of Ehw/P=164.24 are shown in Figure 7. As expected, FSDTC4 shows convergence on the refinement of mesh densities. Also the deflection profile of the shell from FSDTC4 with 900 elements is comparable with the analytical solution [17,22] in Figure 8. From the results, it is found that FSDTC4 is able to give accurate results on the refinement of mesh densities in a pinched cylinder problem.

Example 4: Bending, Vibration and Buckling Analysis of simply supported isotropic square plates

In this example a simply supported isotropic square plate is considered for which CLT results are available for comparison. The boundary conditions are $u_o = w_o = \psi_x = \theta_z = 0$ at $y = 0, a$; $v_o = w_o = \psi_y = \theta_z = 0$ at $x = 0, a$. The following material and geometrical properties are selected: a = 0.5 m, h = variable, E = 68.9 GPa, $\nu = 0.30$. The CLT results for non-dimensional displacement $\left(wD/qa^4\right)$, vibration $\left(\rho\omega^2 ha^4/D\pi^4\right)^{1/2}$ and buckling loads $\left(a^2\sigma_{cr}/D\pi^2\right)$ in

square isotropic plates are 0.00406, 2.0 and 4.0 respectively, which can be found in many text books in the literature. A mesh density of 21 nodes per side in a full plate is employed presently. It is found that a value of shear correction factor $K_{thin} = \frac{K_c^2}{thinparameter} 10^{\left(6K_c^2 - \log 10(thinparameter)\right)}$ $\left(K_c^2 = 5/6\right)$ The thin parameter = (length/thickness ratio) with FSDT4 gives close results with respect to DKT results which we will denote as ECLT4 (equivalent classical four node plate/shell element) henceforth. The results from ECLT4, CLT and FSDTC4 are shown in Figure 9. As seen from the figure, the results from ECLT4 match closely with CLT results for various a/h ratios. The results from FSDTC4 differ significantly from CLT results in thicker regimes and match exactly with the CLT and ECLT4 results for *a/h*=100. Hence it can be concluded that Kirchhoff type elements can be successfully derived from Reissner-Mindlin family of elements with the use of a suitable shear correction factor.

Next, an analytical solution based on the Mindlin plate theory is implemented in a series of steps as mentioned in the many standard text books to analyse bending response of isotropic square plates under uniform transverse loading. The results for the transverse deflection $\left(wD/qa^4\right)$ from the analytical solutions FSDTC, ECLT are compared with the finite element solutions from FSDTC4, ECLT4 and DKT for side to thickness ratios of 10 and 100 are shown in Figure 10. Note that ECLT results are obtained from FSDTC with the inclusion of shear correction factors as mentioned previously. From the figures it is seen that FSDTC4 and ECLT4 are in exact agreement with the solutions from FSDTC, ECLT and DKT for a/h=10 and 100. As seen from the above analytical and FEM results, the Kirchhoff plate theory could be obtained from the Mindlin theory by applying the shear correction factors as mentioned previously.

Example 5: Test for spurious zero energy modes

This example evaluates the free vibration analysis of an isotropic rectangular free-free plate having folded to an angle of 90^o. The free-free boundary conditions are adopted. The following geometrical and material properties are selected [8]: E = 207 GPa, ν = 0.30, ρ=7850 Kg/m^3, h = 0.00121 m. The geometry and mesh density of the rectangular folded plate [8] is shown in Figure 11. For the free-free rectangular folded plate, mesh densities of 5 x2, 10x 4, 20 x 8 in a full plate model are employed in FSDTC4. The present results from FSDTC4 are compared with the experiment [8], FEM [8] and NASTRAN [8] in Table 2. As expected, all the formulations are in excellent agreement with each other on the refinement of mesh densities.

Example 6: Vibration and buckling analysis of composite plates and shells

From an earlier literature review, it is found that there is no result on the transient behaviour of initially stressed laminated composite shells to the best of authors' knowledge. However the analytical results [23] are available for the buckling and vibration analysis of doubly curved laminated composite shells. In this example, present finite element model is compared with the analytical results for validation studies on buckling and vibration behaviour of cross-ply (0/90/0) simply supported doubly curved shells. The boundary conditions are $u_o = w_o = \psi_x = \theta_z = 0$ at $y = 0, b$; $v_o = w_o = \psi_y = \theta_z = 0$ at $x = 0, a$. The thickness and material for all the laminae are the same with the following material properties: For the eigenvibration analysis [23]: $E_1 = 25E_2$, $E_2 = E_3, G_{12} = G_{13} = 0.5E_2$, $G_{23} = 0.5E_2$, $\nu_{12} = \nu_{13} = 0.25$, $\nu_{23} = 0.49$. While for the buckling

analysis [23]: $E_1 = 40E_2$, $E_2 = E_3$, $G_{12} = G_{13} = 0.6E_2$, $G_{23} = 0.5E_2$, $\nu_{12} = \nu_{13} = 0.25$, $\nu_{23} = 0.49$. A mesh density of 21 nodes per side in a full panel is undertaken to obtain the results for FSDTC4, FSDTV4. Note that for FSDTV4, the shear correction factors are calculated from the strain energy approach [14,15]. The comparative results from FSDTV4, FSDTC4 and HSDT [23] (Higher order shear deformation theory), FSDTC [23] and CPT [23] for the non-dimensionalized fundamental frequencies $\left(\bar{\omega} = \sqrt{\frac{\omega^2 a^4 \rho}{E_2 h^2}}\right)$ and critical buckling loads $\left(\bar{N}_{yy} = \frac{N_{yy} a^2}{E_2 h^3}, \bar{N}_{xx} = 0\right)$ for cross-ply (0/90/0) simply supported doubly curved panels are shown in Tables 3 and 4. Close agreement is observed between present and other published results [23].

Example 7: Vibration analysis of folded laminated composite plates

In this example, the natural frequencies of cantilever folded composite plate are examined for which FEM [10-11] results are available. The boundary conditions are $u_o = v_o = w_o = \psi_x = \psi_y = \theta_z = 0$ at x=0. The following material and geometrical properties are employed [10-11]: $E_1 = 60.7GPa$, $E_2 = 24.8GPa$, $G_{12} = G_{13} = G_{23} = 12.0GPa$, $\nu_{12} = 0.23$, ρ=1300 Kg/m^3, L = 20m, L/h = 50. Equal folding length of *L/3* at an angle of 90^o is adopted. The results from a mesh density of 72 elements in full panel are shown in Table 5 along with the results from Niyogi et al [10] and Lee et al [11]. The present results from FSDTC4 and FSDTV4 are in close agreement with previously published results.

Example 8: Transient analysis of laminated composite (0/90) plates

In this example the transient analysis of simply supported laminated folded (180^o angle) composite (0/90) plates under step loading is carried out for which analytical solutions [24] are available. The boundary conditions are : $u_o = w_o = \psi_x = \theta_z = 0$ at $y = 0, b$; $v_o = w_o = \psi_y = \theta_z = 0$ at $x = 0, a$. The following material and geometrical properties are adopted [24]: $E_1 / E_2 = 25$, $E_2 = 2.1\times10^6 N/cm^2$, $\nu_{12} = 0.25$, $G_{12} = G_{13} = 0.5E_2$, $G_{23} = 0.2E_2$, $\rho = 8\times10^{-6} N - s^2/cm^4$, *a/b*=1, *a*=25 cm, *a/h*=10, $q_o = 1\times10^6 N/cm^2$ .The FSDTC4 results for the central displacement $\left(wE_2h^3100/b^4q_o\right)$, fundamental frequency $\left(\sqrt{\left(\omega^2a^4\rho/E_2h^2\right)}\right)$ are 1.9455, 8.9169, whereas the corresponding analytical solutions are 1.947 and 8.900. The results for nondimensional central displacement $\left(wE_2h^3100/b^4q_o\right)$ and central stress $\left(\sigma_{yy}h^2/b^2q_o\right)$ at (*x=a/2, b=b/2, z=h/2*) from the present formulation FSDTC4 are compared with the analytical solutions from FSDTC [24] in Figures 12 and 13.

As seen from the Figures 12 and 13, the present results are in close agreement with earlier published results from the literature.

Example 9: Transient analysis of laminated folded composite $(0/90/0/90/0)_s$ plates

In this example, transient analysis of laminated composite folded (with 90^o and 180^o angles) composite *$(0/90/0/90/0)_s$* plates is performed. The following material and geometrical properties are employed [25]: E_1 = 128 GPa, E_2 = 11 GPa, $G_{12} = G_{13}$ =4.48 GPa, G_{23} =1.53 GPa, ν_{12} = 0.25, ρ = 1500 Kg/m^3, ply thickness=0.0013 m, $a = b$ = 1.8 m (for 180^o folded plates and shells) and

$a = b = 2$ m (for folded plates). For 180^o folded plates and spherical shells ($R/a = 10$), a mesh density of 19 nodes per side in a full plate and shell model is taken, whereas a mesh density of 13 nodes per side in a full plate model is taken for a 90^o folded plate. The edges of 180^o folded plates and shells are simply supported, whereas two opposite folded sides of the 90^o folded plates are clamped. The following boundary conditions are adopted in the analysis: Simply supported (S) (for cross ply): $u_o = w_o = \psi_x = \theta_z = 0$ at $y = 0, b$; $v_o = w_o = \psi_y = \theta_z = 0$ at $x = 0, a$; Clamped (C); $u_o = v_o = w_o = \psi_x = \psi_y = \theta_z = 0$ at $x = 0, a$. Note that the uniform step load of 10^6 N/m^2 acts on an area of $x = a/3$ and $y = b$ of the middle part of the plates and shells. A time step of 2 micro seconds is taken in the Newmark integration scheme. Note that for this particular problem, both FSDTC4 and FSDTV4 yield similar results due to thin panels. The results for central displacement $\left(wE_2h^3100/a^4q_o\right)$ under an initial pre-stress of -0.5 N_{ycr} subjected to step loading are shown in Figures 14 and 15. It is seen from the Figure 14 that the response from shell panel is lower as compared to plate panel due to curvature effects. Figure 14 results could serve benchmark for carrying out analytical solutions based on Navier type solutions. Figure 15 results could serve benchmark for Rayleigh-Ritz type solutions for 90^o folded plates with two opposite sides clamped and two opposite sides free edge conditions.

Example 10: Transient analysis of laminated folded composite sandwich (0/90/0/90/Core)$_s$ plates

In this example, transient analysis of laminated composite folded (90^o angle) composite sandwich plates is performed. The two opposite folded sides of the 90^o folded plates are clamped. The following boundary conditions are adopted in the analysis: Clamped (C);

$u_o = v_o = w_o = \psi_x = \psi_y = \theta_z = 0$ at $x = 0, a$. The material properties of the face plate are same as those of the previous example.

For core, the following material properties [24] are taken: E_1=0.10363 GPa, ν_{12} = 0.32, G_c = 0.050 GPa, ρ_c = 130 Kg/m^3, h_c (Core thickness) = 0.117m. *a/b* = 1, *a* = 2.0m. The transverse load on an area of *a/3* and *b* is given by $q_o F(t)$ where *F(t)* is for step loading: 1 for $0 < t > t_1$ and 0 for $t > t_1$., t_1 = 0.016 sec and $q_o = 10^6$ N/m^2. A time step of 40 micro seconds is taken in the Newmark integration scheme. A mesh density of 13 nodes per side in a full plate model is taken. Effects of various prestress ($0.0N_{ycr}$, $1.0N_{ycr}$ and $-0.5N_{ycr}$ are shown in Figure 16 and the effects of laminate orientations $(0/\theta/0/\theta/0/core)_s$ with varying θ=0, 45 and 90 are shown in Figure 17. From Figure 16, it is found that due to compressive nature of the prestress, the folded plate panel shows higher response as compared to Null and tensile prestress. From Figure 17, it is found that the skin stacking sequence with all 0^o orientations gives higher response than angular orientations due to the trade off effects between stiffness, mass and buckling matrices.

4 Concluding Remarks

A four node assumed strain vortex shell element is developed on the basis of a first order shear deformation theory with C^o continuity requirements to study the transient analysis of initially stressed folded composite sandwich plate structures. Consistent mass matrix is employed to preserve the total kinetic energy of the system. Full integration is carried out to integrate various terms in the energy formulation to make the procedure very clean. Conventional degrees of freedom is maintained which are fully standard. A wide variety of problems are studied to assess the behaviour of a four node shell element. Numerical results are presented for transient

analysis of composite plates and shells. It is hoped that these studies could provide great motivations to carry out folded plate analysis for which very few studies are available, in future.

References

[1] Qatu, M.S, 2002. Recent Advances in the Dynamic Behaviour of Shells: 1989-2000, Part 1: Laminated Composite Shells, *Applied Mechanics Reviews, Trans. Of ASME*, Vol. 55, pp.325-350.

[2] Yang, H.T.Y., Saigal, S., Masud, A., Kapania, R.K., 2000, A Survey of Recent Shell Finite Elements, *International Journal for Numerical Methods in Engineering*, Vol.47, pp.101-127.

[3] Mackerle, J., 2002, Finite Element Analysis of Sandwich Structures: A Bibliography (1980-2001), *Engineering Computations*, Vol. 19, pp.206-245.

[4] Irie, T., Yamada, G., Kobayashi, Y., 1984, Free Vibration of a Cantilever Plate, *Journal of Acoustical Society of America*, Vol 76, pp.1743-1748.

[5] Liu, W.H., Huang, C.C., 1992, Vibration Analysis of Folded Plates, *Journal of Sound and Vibration*, Vol. 157, pp.123-137.

[6] Cheung, Y.K., Kong, J., 1995, Vibration and Buckling of Thin Walled Structures By a New Finite Strip, *Thin Walled Structures*, Vol. 21, pp.327-343.

[7] Daniel, A.N., Doyle, J.F., Rizzi, S.A., 1996, Dynamic Analysis of Folded Plate Structures, *Journal of Vibration and Acoustics, Trans. ASME*, Vol. 118, pp.591-598.

[8] Allman, D.J., 1996, Implementation of a Flat Facet Shell Finite Element For Applications in Structural Dynamics, *Computers and Structures*, Vol. 59, pp.657-663.

[9] Suresh, R., Malhotra, S.K., 1998, Vibration and Damping Analysis of Thin-Walled Box Beams, *Journal of Sound and Vibration*, Vol. 215, pp.201-210.

[10]Niyogi, A.G., Laha, M.K., Sinha, P.K., 1999, Finite Element Vibration Analysis of Laminated Composite Folded Plate Structures, *Shock and Vibration*, Vol. 6, pp.273-283.

[11]Lee, S.Y., Wooh, S.C., Yhim, S.S., 2004, Dynamic Behaviour of Folded Composite Plates Analysed By The Third Order Plate Theory. *International Journal of Solids and Structures*, Vol. 41, pp.1879-1892.

[12]Lee, S.Y., Wooh, S.C., 2004, Finite Element Vibration Analysis of Composite Box Structures Using The High Order Plate Theory., *Journal of Sound and Vibration,* Vol. 277, pp.801-814.

[13]Rao, V.S., Shankar, B.V., Sun, C.T., 1992, Constrained Layer Damping of Initially Stressed Composite Beams Using Finite Elements, *Journal of Composite Materials,* Vol. 26, pp.1-12.

[14]Nayak, A.K., Shenoi, R.A., 2004, Assumed Strain Shell Elements For Damped Composite Sandwich Shells, *Proceedings of the 1st International Congress of Computational Mechanics and Simulation, ICCMS04,* IIT Kanpur, 9-12th December 2004.

[15]Nayak, A.K., Shenoi, R.A., 2005, Free Vibration Analysis of Composite Sandwich Shells Using Assumed Strain Higher Order Shell Elements, *AIAA-2005-1837,46th AIAA/ASME/ASCE/AHS/ASC Structures, Structural Dynamics and Materials Conference 13th AIAA/ASME/AHS Adaptive Structures Conference* 7t, Austin, Texas, April 18-21, 2005.

[16]Cook, R.D., 1994, Four Node Flat Shell Element-Drilling Degrees of Freedom, Membrane Bending Coupling, Warped Geometry, and Behavior, *Computers and Structures*, Vol. 50, pp.549-555.

[17]Dvorkin, E.N., Bathe, K.J., 1984, A Continuum Mechanics Based Four-Node Shell Element For General Non-linear Analysis, *Engineering Computations,* Vol. 1, pp.77-88.

[18] Vlachoutsis, S., 1992, Shear Correction Factors for Plates and Shells, *International Journal for Numerical Methods in Engineering*, Vol. 33, pp.1537-1552.

[19] Kant, T., Khare, R.K., 1997, A higher order facet quadrilateral composite shell element, *International Journal for Numerical Methods in Engineering*, Vol. 40, pp.4477-4499.

[20]Kebari, H., Cassell, A.C., 1991, Stabilization by Non-conforming Modes: 9-node Membrane Element With Drilling Freedom, *International Journal for Numerical Methods in Engineering*, Vol. 31, pp.1453-1468.

[21]Gibson, J.E., 1961, The Design of Cylindrical Shell Roofs*, Spon*, London.

[22]Fl*ü* gge, W., 1973, Stresses in Shells, 2nd Edition, *Springer-Verlag*, Berlin.

[23]Librescu, L., Khdeir, A.A., Frederick, D., 1989, A Shear Deformable Theory of Laminated Composite Shell Type Panels and Their Response Analysis, I: Free Vibration and Buckling, *Acta Mechanica*, Vol. 76, pp.1-33.

[24]Reddy ,JN. Mechanics of Laminated Composite Plates and Shells, Theory and Analysis, 2004, Second Edition, CRC Press.

[25] Nayak AK, Shenoi RA and Moy SSJ, 2006, Dynamic response of composite sandwich plates subjected to initial stresses, Composites Part A- Applied Science and manufacturing, Vol 37, pp.1189-1205.

List of Figures

Figure 1: Typical geometry of a composite sandwich shell with local and global co-ordinate systems

Figure 2: Sampling positions for shear interpolation in the 4 node assumed strain element (a) $\bar{\varepsilon}_{\xi\varsigma}^{sij}$ (b) $\bar{\varepsilon}_{\eta\varsigma}^{sij}$

Figure 3: Barrel Vault Shell Problem; R=300, L=600, h=3.0, E=3.0 x 10^6, ν=0.0, specific weight=0.208333.

Figure 4: Convergence of FSDTC4 element with Barrel-Vault shell problem; Deep shell solution=3.6288, Shallow shell solution=3.7033, Normalised with respect to Deep shell solution 3.6288.

Figure 5: The displacement profile of the Barrel-vault Shell roof; Analytical o, FSDTC4 -

Figure 6: Pinched cylinder problem; R=300, L=600, h=3.0, E=3.0x 10^6, ν=0.30, P=1.0

Figure 7: Convergence of FSDTC4 element in pinched-cylinder problem; Normalised with respect to 164.24.

Figure 8: Deflected profile of the pinched cylindrical shell, Analytical=o, and FSDTC4 -

Figure 9: Comparison of various formulations for simply supported isotropic plates under uniform loading; a) ECLT (a/h=10) (dashed) and FSDTC (a/h=10) (solid), b) ECLT (a/h=100) (dashed) and FSDTC (a/h=100) (solid), c) ECLT4 (a/h=10) (dashed) and FSDTC4 (a/h=10) (solid), d) ECLT4 (a/h=100) (dashed) and FSDTC4 (a/h=100) (solid), e) DKT (a/h=10) (dashed) and ECLT (a/h=10) (solid), f) DKT (a/h=100) (dashed) and ECLT (a/h=100) (solid)

Figure 10: Comparison of various formulations for transverse deflection $\left(wD/qa^4\right)$ of simply supported isotropic plates under uniform loading (q); a) ECLT (a/h=10) (dashed) and FSDTC (a/h=10) (solid), b) ECLT (a/h=100) (dashed) and FSDTC (a/h=100) (solid), c) ECLT4 (a/h=10)

(dashed) and FSDTC4 (a/h=10) (solid), d) ECLT4 (a/h=100) (dashed) and FSDTC4 (a/h=100) (solid), e) DKT (a/h=10) (dashed) and ECLT (a/h=10) (solid), f) DKT (a/h=100) (dashed) and ECLT (a/h=100) (solid)

Figure 11: Allman's folded plate problem

Figure 12: Transient analysis of laminated composite plate under step loading

Figure 13: Transient analysis of laminated composite plate under step loading

Figure 14: Transient analysis of laminated composite plates and shells under step loading

Figure 15: Transient analysis of laminated composite folded plate under step loading

Figure 16: Transient analysis of laminated composite sandwich folded plate under step loading

Figure 17: Effect of laminate orientations on transient analysis of laminated composite sandwich folded plate under blast loading

List of Tables

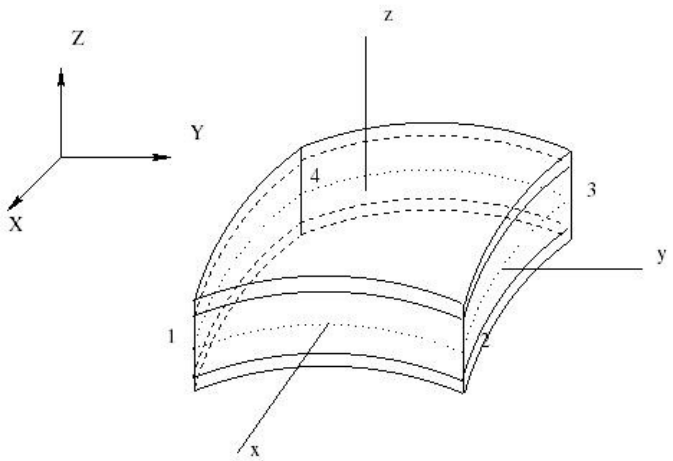

1

Figure 1:

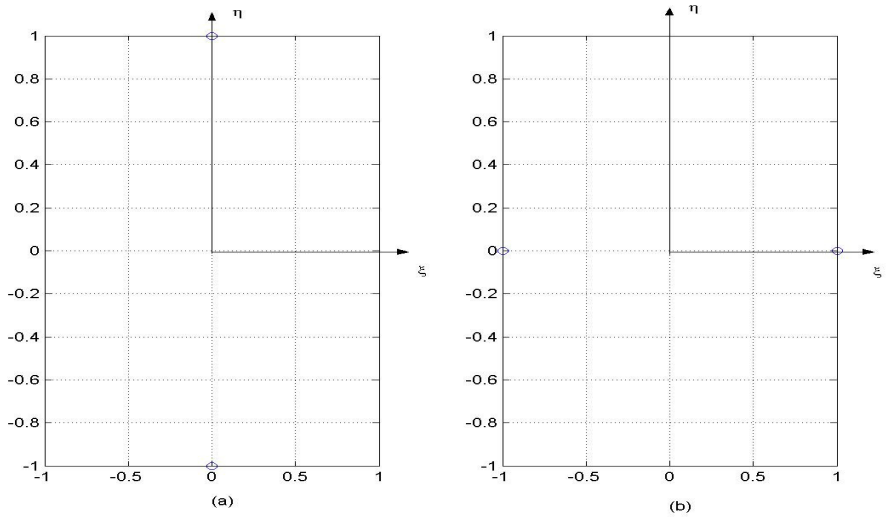

Figure 2:

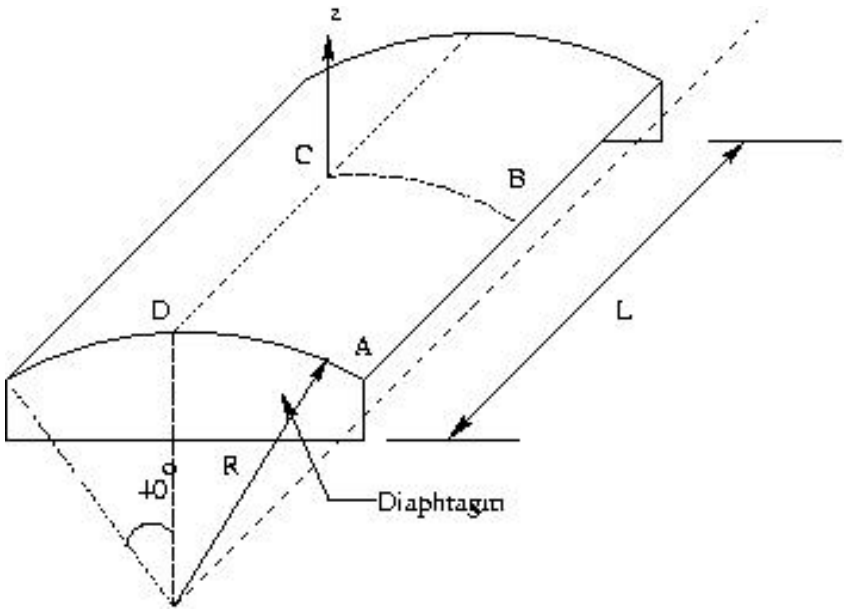

Figure 3:

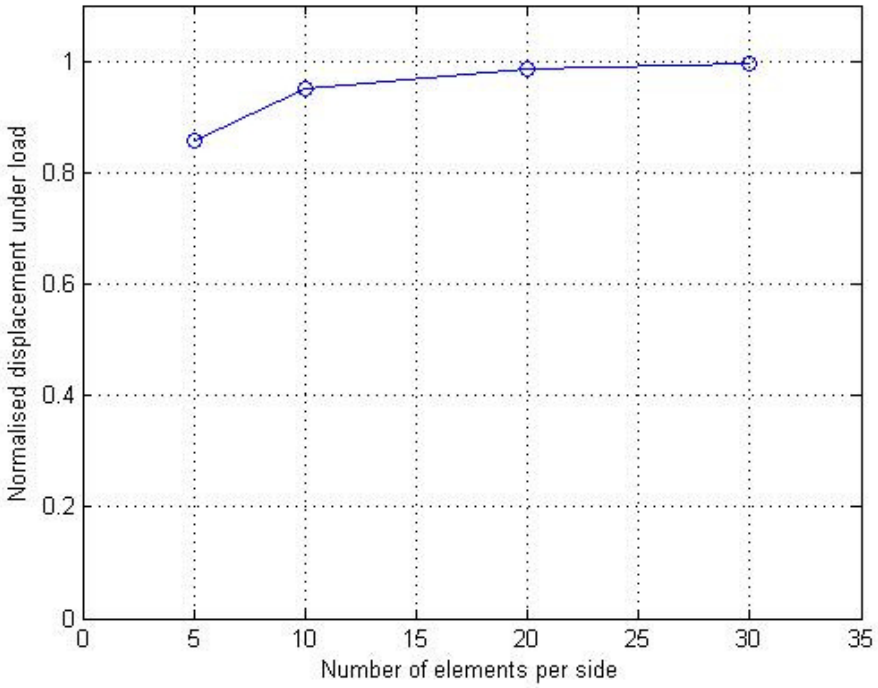
Normalised displacement under load
Number of elements per side
0
0.2
0.4
0.6
0.8
1
0
5
10
15
20
25
30
35

Figure 4:

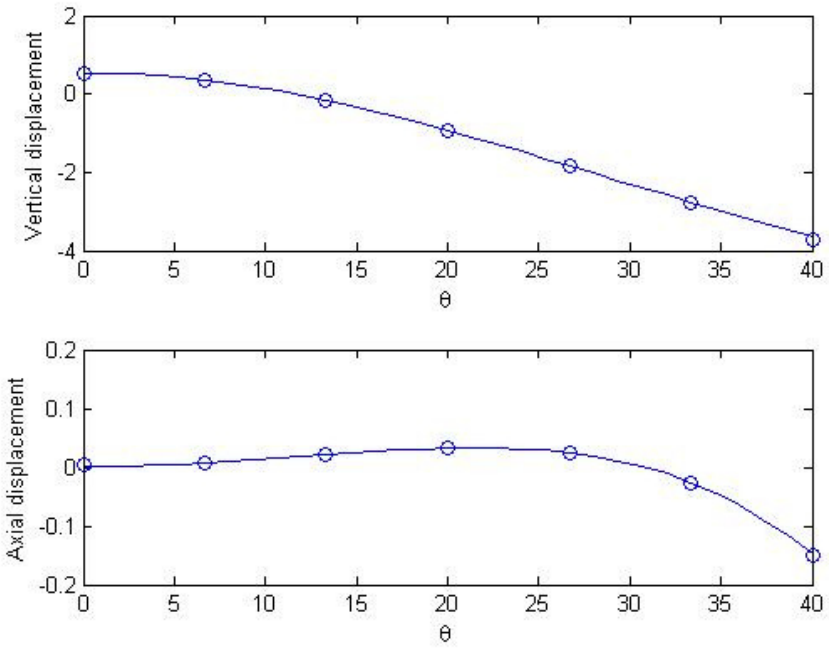
Vertical displacement
2
0
-2
-4
0
5
10
15
20
25
30
35
40
θ
Axial displacement
0.2
0.1
0
-0.1
-0.2
0
5
10
15
20
25
30
35
40
θ

Figure 5:

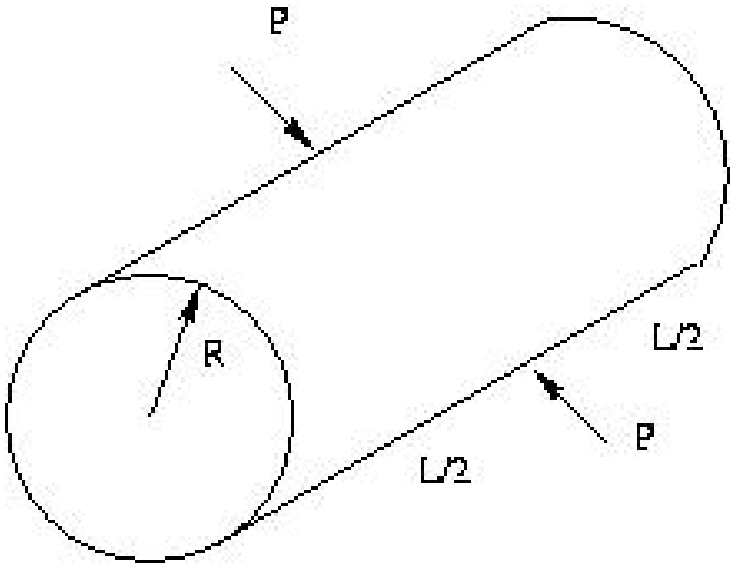

Figure 6:

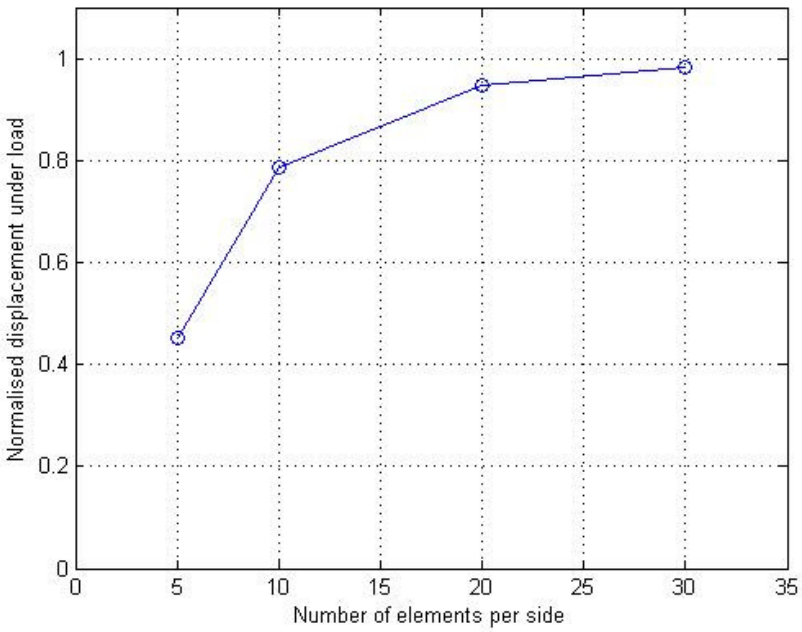
Normalised displacement under load
Number of elements per side
0
0.2
0.4
0.6
0.8
1
0
5
10
15
20
25
30
35

Figure 7:

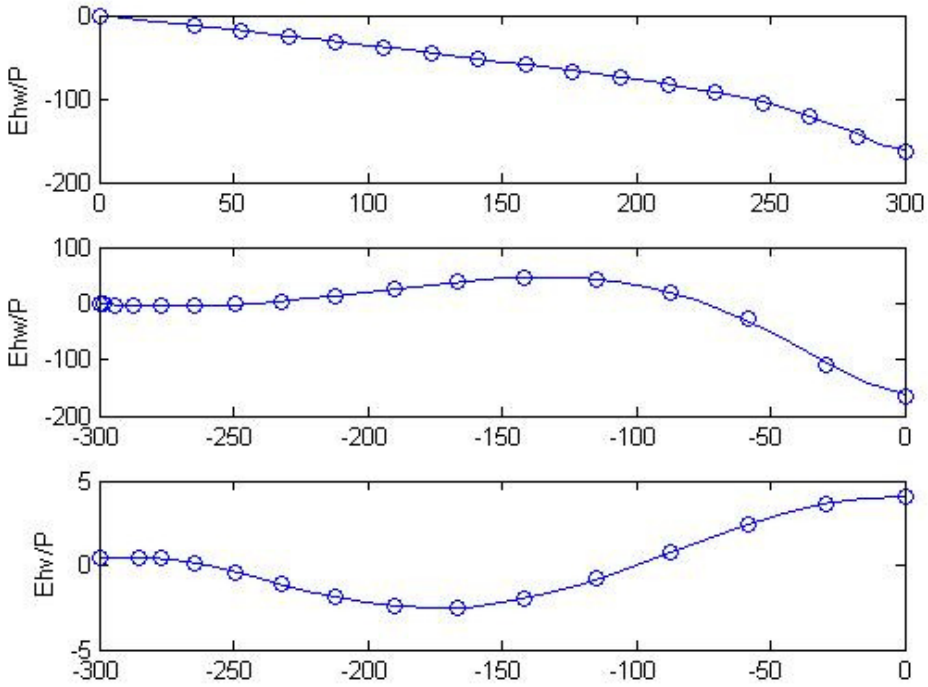
Ehw/P
0
-100
-200
0
50
100
150
200
250
300
Ehw/P
100
0
-100
-200
-300
-250
-200
-150
-100
-50
0
Ehw/P
5
0
-5
-300
-250
-200
-150
-100
-50
0

Figure 8:

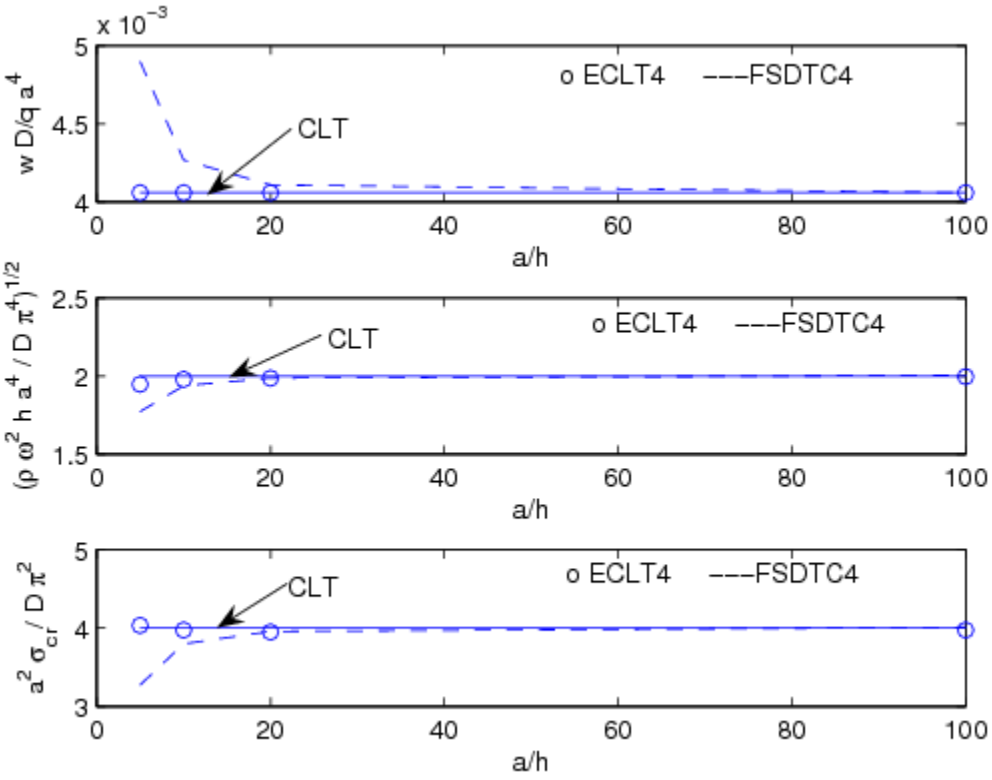
x 10^-3
w D/q a^4
o ECLT4
---FSDTC4
CLT
a/h
(ρ ω^2 h a^4 / D π^4)^1/2
o ECLT4
---FSDTC4
CLT
a/h
a^2 σ_cr / D π^2
o ECLT4
---FSDTC4
CLT
a/h

Figure 9:

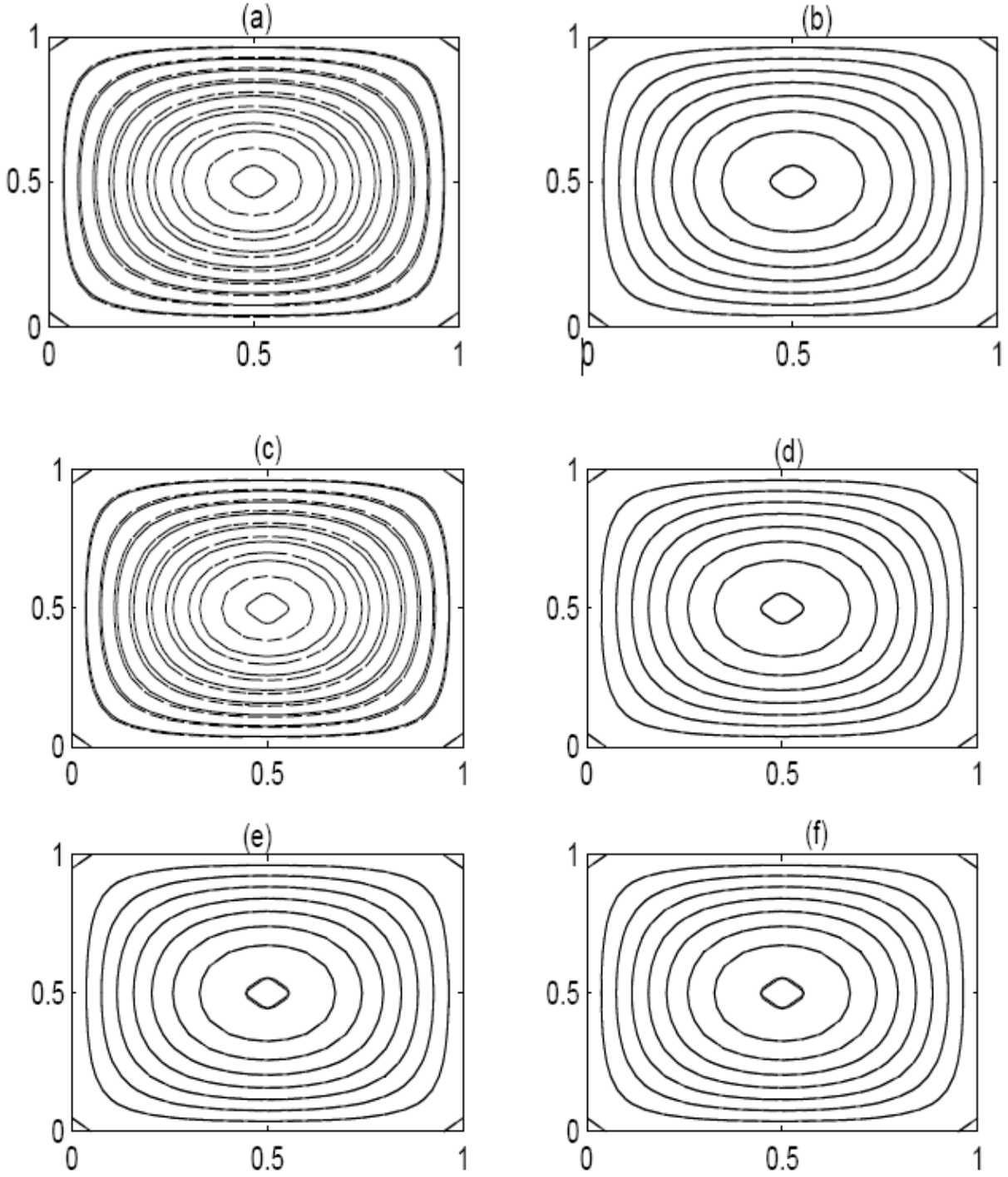

Figure 10:

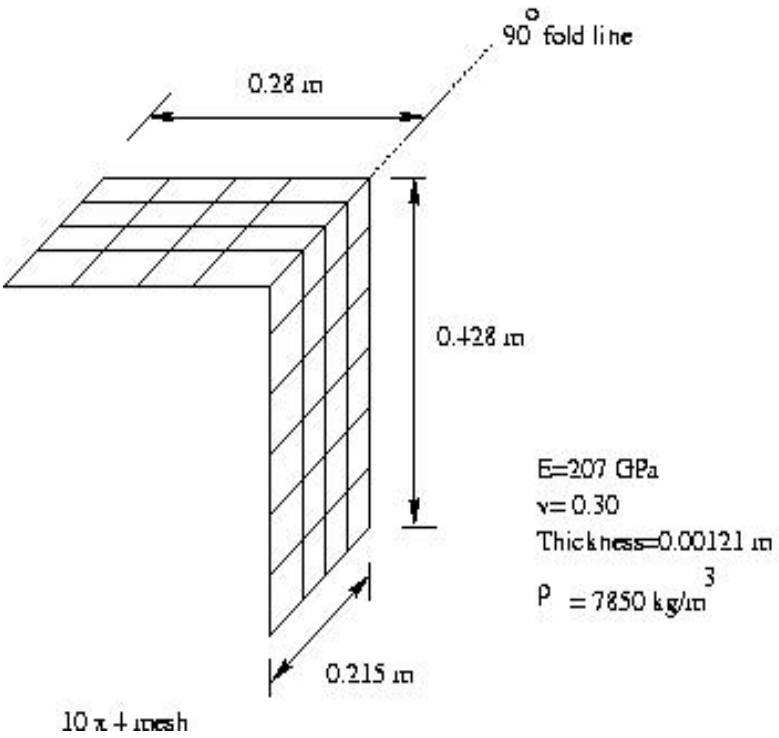
90° fold line
0.28 m
0.428 m
E=207 GPa
ν= 0.30
Thickness=0.00121 m
ρ = 7850 kg/m3
0.215 m
10 x 4 mesh

Figure 11:

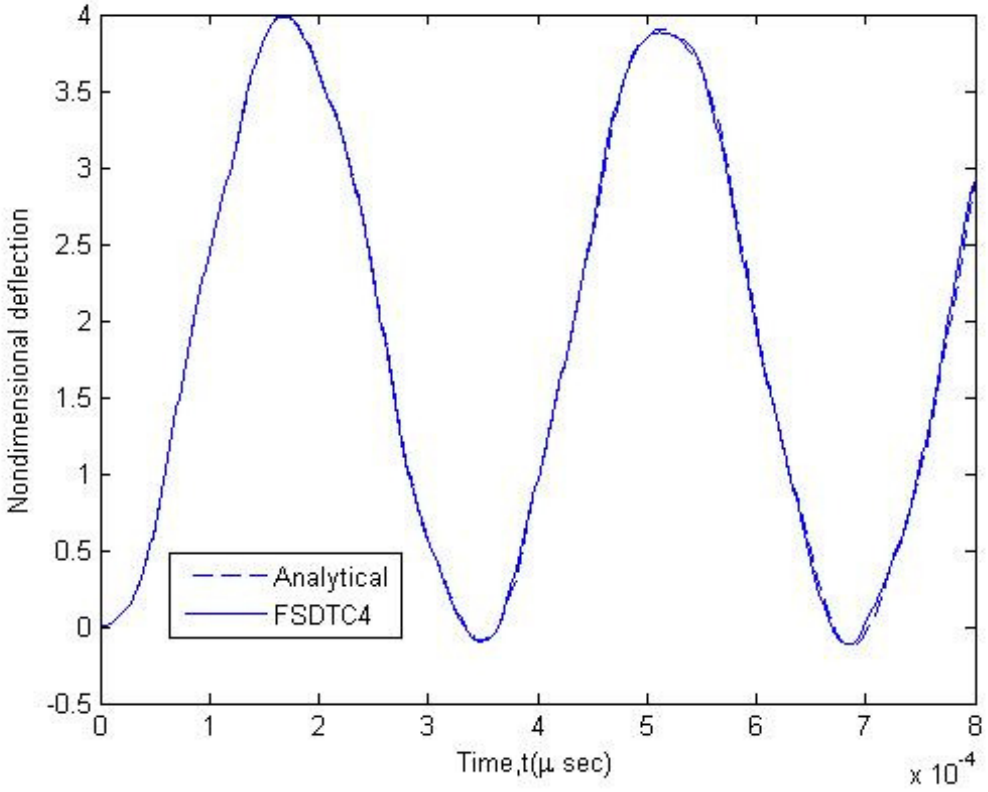
Nondimensional deflection
Time,t(μ sec)
x 10^-4
Analytical
FSDTC4
4
3.5
3
2.5
2
1.5
1
0.5
0
-0.5
0
1
2
3
4
5
6
7
8

Figure 12:

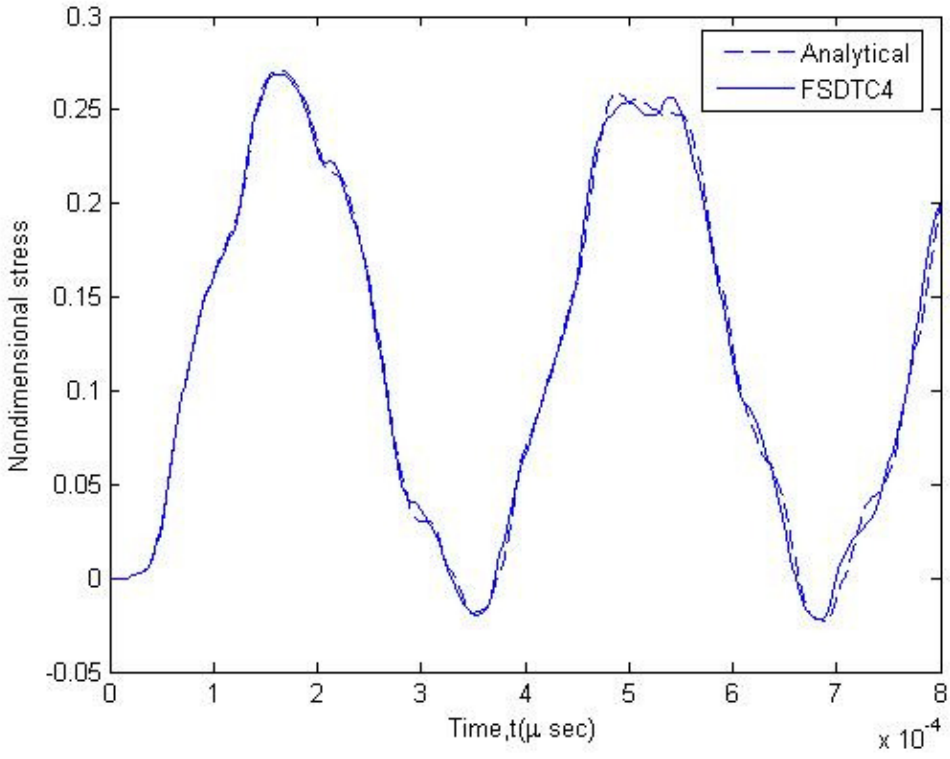
Analytical
FSDTC4
Nondimensional stress
Time,t(μ sec)
x 10^-4
0.3
0.25
0.2
0.15
0.1
0.05
0
-0.05
0
1
2
3
4
5
6
7
8

Figure 13:

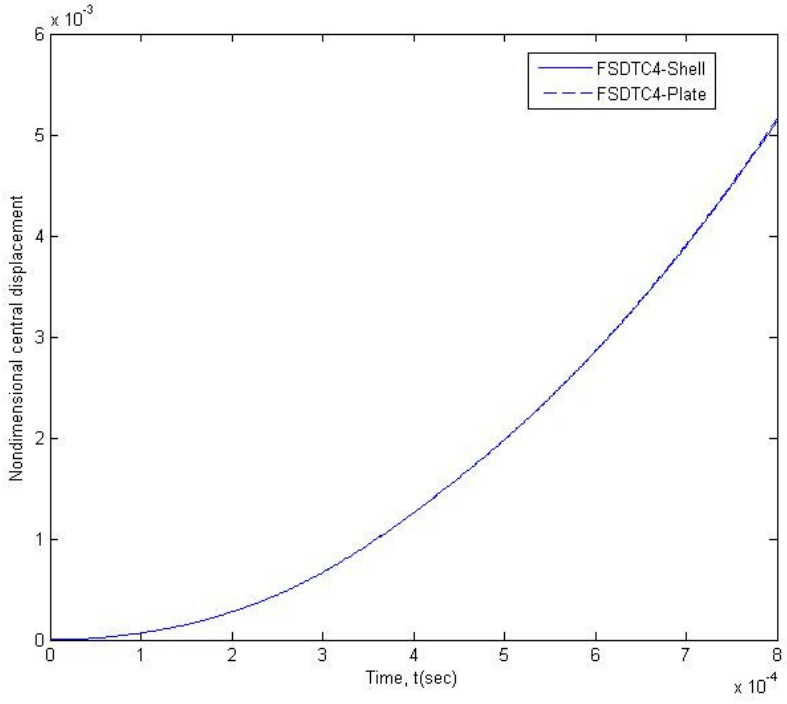
x 10^-3
6
5
4
3
2
1
0
Nondimensional central displacement
FSDTC4-Shell
FSDTC4-Plate
0
1
2
3
4
5
6
7
8
Time, t(sec)
x 10^-4

Figure 14:

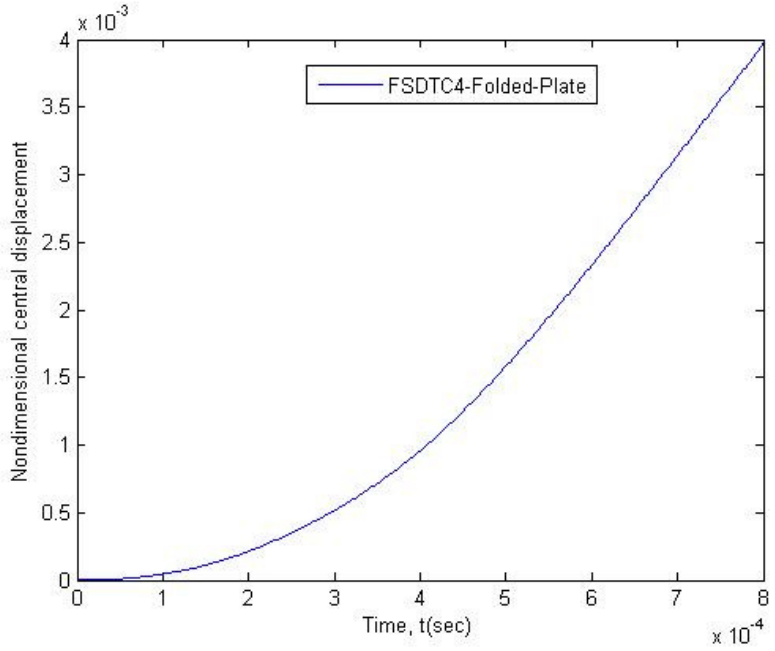
x 10^-3
4
3.5
3
2.5
2
1.5
1
0.5
0
Nondimensional central displacement
FSDTC4-Folded-Plate
0
1
2
3
4
5
6
7
8
Time, t(sec)
x 10^-4

Figure 15:

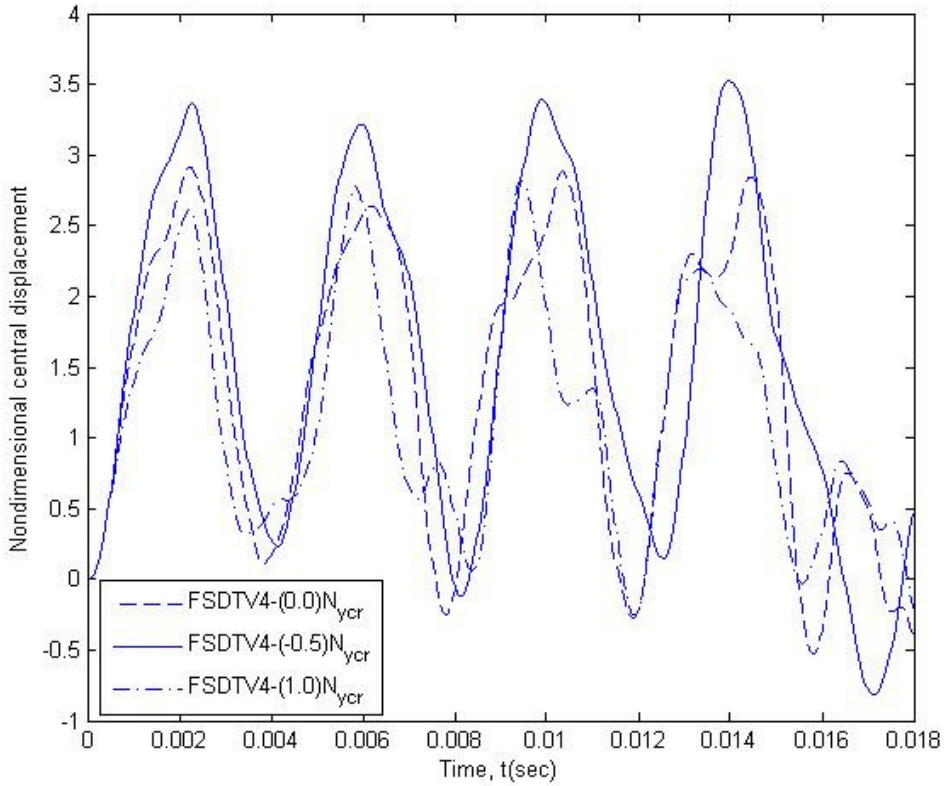
Nondimensional central displacement
Time, t(sec)
FSDTV4-(0.0)N_ycr
FSDTV4-(-0.5)N_ycr
FSDTV4-(1.0)N_ycr
4
3.5
3
2.5
2
1.5
1
0.5
0
-0.5
-1
0
0.002
0.004
0.006
0.008
0.01
0.012
0.014
0.016
0.018

Figure 16:

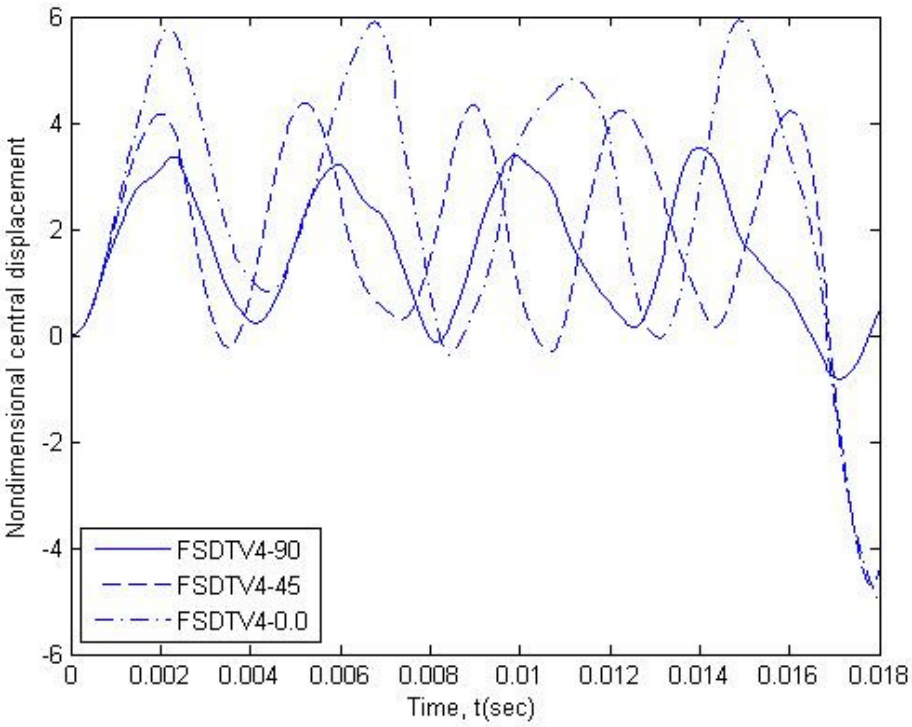
Nondimensional central displacement
Time, t(sec)
FSDTV4-90
FSDTV4-45
FSDTV4-0.0
6
4
2
0
-2
-4
-6
0
0.002
0.004
0.006
0.008
0.01
0.012
0.014
0.016
0.018

Figure 17:

Mesh	4x1	8x2	16x4	20x5	24x6	32x8
Displacement	0.32833	0.34791	0.35403	0.35486	0.35533	0.35583

Table 1:

Source	Mode 1	Mode 2	Mode 3	Mode 4
Expt[8]	10.49	25.24	32.24	36.44
FEM[8]	10.73	24.85	32.99	38.80
FEM[8]	10.46	23.85	31.66	37.48
NASTARN[8]	10.42	23.15	31.40	35.53
FSDTC4(5x2)	11.01	25.13	39.32	40.12
FSDTC4(10x4)	10.82	24.79	34.21	38.40
FSDTC4(20x8)	10.81	24.69	32.94	37.93

Table 2:

R_1/a	R_2/b	HSDT[21]	FSDTC[21]	CPT[21]	FSDTV	FSDTC
5	5	12.200	12.394	15.290	11.689	12.439(0.36)**
10	5	12.096	12.296	15.206	11.566	12.327(0.25)
10	20	11.990	12.193	15.129	11.456	12.227(0.28)
20	20	11.973	12.178	15.116	11.433	12.207(0.24)
10^{30}	10^{30}	11.958	12.163	15.104	11.416	12.191(0.23)

**Numbers in the parenthesis indicate the errors with respect to FSDTC analytical results.

Table 3:

R_1/a	R_2/b	HSDT[21]	FSDTC[21]	CPT[21]	FSDTV	FSDTC
5	5	13.154	13.072	18.726	12.368	13.163(0.70)**
10	5	12.940	12.865	18.505	12.141	12.936(0.55)
10	20	12.891	12.818	18.450	12.103	12.902(0.66)
20	20	12.844	12.773	18.402	12.053	12.852(0.62)
10^{30}	10^{30}	12.824	12.753	18.380	12.032	12.832(0.62)

**Numbers in the parenthesis indicate the errors with respect to FSDTC analytical results.

Table 4:

Source	$(30/-30)_s$	$(0/90)_s$	$(0/90)_2$
Niyogi et al [10]	0.0901	0.0896	0.0987
Lee et al [11]	0.0925	0.1055	0.0982
FSDTC4	0.0913	0.0897	0.0999
FSDTV4	0.0913	0.0897	0.0999

Table 5: